Sensitive Broadband ELF/VLF Radio Reception With the AWESOME Instrument

Morris B. Cohen, *Member, IEEE*, Umran S. Inan, *Fellow, IEEE*, and Evans W. Paschal

***Abstract*—A new instrument has been developed and deployed for sensitive reception of broadband extremely low frequency (ELF) (defined in this paper as 300–3000 Hz) and very low frequency (VLF) (defined in this paper as 3–30 kHz) radio signals from natural and man-made sources, based on designs used for decades at Stanford University. We describe the performance characteristics of the Atmospheric Weather Electromagnetic System for Observation, Modeling, and Education (AWESOME) instrument, including sensitivity, frequency and phase response, timing accuracy, and cross modulation. We also describe a broad range of scientific applications that use AWESOME ELF/VLF data involving measurements of both subionospherically and magnetospherically propagating signals.**

***Index Terms*—Amplifiers, analog circuits, broadband amplifiers, ionosphere, lightning, low-frequency (LF) radio, magnetosphere, radio receivers, remote sensing, waveguide antennas.**

I. Introduction

THE ANALYSIS of radio waves of extremely low frequencies (ELF) (defined in this paper as 300 Hz–3 kHz) and very low frequencies (VLF) (defined in this paper as 3–30 kHz) is useful for studying the dynamics of the Earth's ionosphere and magnetosphere as well as subterranean imaging and global communications and navigation. For instance, lightning radiates the bulk of its electromagnetic energy in the ELF/VLF frequency range [1, p. 118], launching signals known as radio atmospherics (or sferics) which are almost entirely reflected at the D region (70–90 km altitude) of the ionosphere. These signals (like others in this frequency range) are efficiently guided to global distances in the so-called Earth-ionosphere waveguide. Attenuation rates are typically only a few decibels per megameter [2, p. 389] after the first $\sim$500 km for waveguide mode structure to be established. Propagation characteristics in the Earth-ionosphere waveguide are in general a strong function of the ionospheric conditions, which leads to dramatically different propagation characteristics between daytime and nightime. In addition, some of the ELF/VLF energy leaks upward in the plasma whistler mode to the magnetosphere, where it can strongly impact the electron dynamics of the Van Allen radiation belts and can be received in the geomagnetic conjugate region [3]. Natural ELF/VLF signals known as chorus and hiss can also be generated *in situ* in the magnetosphere, particularly at mid and high geomagnetic latitudes, as a result of the interaction between energetic electrons in the radiation belts and ELF/VLF whistler-mode waves (see [4], and references therein). Due to the long-distance propagation of ELF/VLF waves, as well as the relatively deep (10 s of meters skin depth) penetration of ELF/VLF waves into seawater, a number of VLF transmitters operate at frequencies between 10 and 60 kHz for naval communication with surface ships and submerged submarines. A global collection of such transmitters has also been used for accurate navigation via phase-coherent triangulation, such as the so-called "Omega" system [5]. Because ELF/VLF propagation is strongly influenced by D-region ionospheric conditions, these VLF transmitter signals are also used to remotely sense ionospheric disturbances resulting from different physical processes. Moreover, because of the relatively high (hundreds of meters, due to the skin effect) penetration into the Earth, ELF/VLF waves are a useful tool for subterranean prospecting and imaging [6].

The first observations of natural signals at ELF and VLF frequencies were made serendipitously in the late 19th and early 20th century, when these signals audibly coupled into long telephone and transmission lines [7, p. 11]. The first uses of ELF/VLF waves for long-distance communications came as a result of Giglielmo Marconi's pioneering experiments from 1901 to 1904, which led to the establishment of the first transatlantic communications. Research on ELF/VLF signals grew rapidly in the 1950s, spurred on in part by the International Geophysical Year of 1957. During this period, theories of whistler propagation in the Earth's magnetoplasma were developed first by L. R. O. Storey [7, p. 17]. In parallel, understanding of the propagation of waves in the Earth-ionosphere waveguide came from the experimental observations of lightning-generated radio atmospherics (or "sferics") [8] and theoretical development of the quantitative theory of ELF and VLF propagation [9], [10].

These early observations motivated, and consequently were driven by, advances in hardware and equipment for detection of these ELF/VLF signals. Potter [11] used sound and

Manuscript received March 13, 2009; revised April 30, 2009 and May 18, 2009. This work was supported in part by the Center for Integrated Space Weather Modeling, National Science Foundation, Boston, by the Defense Advanced Research Projects Agency and Air Force Research Laboratory under an Office of Naval Research (ONR) Grant N00014-09-1, by ONR under Grant N00014-06-1-1036 to Stanford University, by the International Heliophysical Year Program under a National Aeronautics and Space Administration Grant NNX07AM21G, with shared costs by Stanford University, and by the Air Force Office of Scientific Research (AFOSR) under AFOSR Grant FA9550-06-1-0519.

M. B. Cohen is with the Space, Telecommunications, and Radioscience Laboratory, Department of Electrical Engineering, Stanford University, Stanford, CA 94305 USA (e-mail: morris.cohen@gmail.com).

U. S. Inan is with the Department of Electrical Engineering, Stanford University, Stanford, CA 94305 USA, and also with the Koç University, Istanbul 34450, Turkey (e-mail: inan@stanford.edu).

E. W. Paschal is with the Whistler Radio Services, Anderson Island, WA 98303 USA (e-mail: epaschal@att.net).

Color versions of one or more of the figures in this paper are available online at http://ieeexplore.ieee.org.

Digital Object Identifier 10.1109/TGRS.2009.2028334

speech analysis techniques to present the first frequency–time spectrograms of ELF/VLF radio data, followed by L. R. O Storey's use of a spectrum analyzer [7, p. 19]. The development of magnetic-tape recordings enabled archiving and postanalysis for the first time [7, p. 16]. In the early 1960s, Vanguard III, Injun, and Allouette became the first satellites to record whistlers and other whistler-mode waves in the magnetosphere [7, p. 308].

Initially, ELF/VLF receivers required large aerials or loops of wire (to detect the wave magnetic field) to achieve sufficient sensitivity. For instance, the so-called "IGY" antenna size was a right isosceles triangle, 45-ft base and 22.5-ft height. Paschal [12] discusses ELF/VLF receiver design using air-core wire loops, with a low-noise amplification system consisting of an impedance-matching transformer, and discrete transistor amplification, which forms the basis of the receiver design used hereinafter. The design therein enabled a family of antennas with the same impedance to be utilized with the same receiver, enabling either portability or high sensitivity, depending on the size chosen. The analysis by Paschal [12] concludes that over 1.5–2 decade range of frequencies, a sufficiently low-noise receiver can be implemented such that the primary limiting factor to ELF/VLF sensitivity is the thermal noise of the resistance of wire loop. By comparing the rms value of this thermal noise to the induced voltages from magnetic fields, Paschal [12] concludes that the sensitivity of transformer-matched antenna and receiver system (i.e., the lowest magnetic field value that can be detected for a given bandwidth) can be written as inversely proportional strictly to $\sqrt{AM}$, where A is the area inside the wire loop and M is the mass of the metal wires, a relationship first noted by R. H. Rorden.

Stanford University has been operating ELF/VLF receivers since the 1950s, beginning with the observations of sferics at Stanford University and, later, simultaneous observations aboard a ship at the conjugate magnetic location [13]. The Siple Station, Antarctica, VLF transmitter experiment involved construction of 21-km-long crossed dipole [14] for controlled excitation of whistler-mode signals into the magnetosphere [3]. For this purpose, ELF/VLF receivers were placed both at Siple, as well as the conjugate magnetic location in northeastern Canada, where so-called "magnetospheric one-hop" signals were measured [15]. Data were recorded onto magnetic tape, and techniques were then developed to extract phase information despite the limitations of magnetic-tape recordings [16].

In another effort, the Stanford radiometer operated over 16 different frequency ranges between 10 Hz and 32 kHz [17] to clearly detect the rms background-noise environment, enabling long-term studies of natural ELF/VLF radio noise [18], [19].

In recent decades, Stanford ELF/VLF receiver systems included real-time digitization of data on-site, rather than storing them on magnetic tape or chart paper. This metamorphosis has been greatly aided by advances in computing resources for on-site processing (such as real-time coherent demodulation and extraction of amplitude and phase of VLF transmitter signals) and data archiving (via DVDs and other large-scale media storage devices). The advent of the global positioning system (GPS) has enabled timing accuracy sufficient for interferometric measurements between sites and precise coherent extraction of phase information from narrowband signals, without the use of expensive and carefully tuned stable local oscillators. Finally, the proliferation of circuit-board design techniques has enabled faster prototyping and easy reproduction or updating of design iterations.

The Atmospheric Weather Electromagnetic System for Observation, Modeling, and Education, or AWESOME receiver, builds on the decades of legacy in construction and operation of ELF/VLF receivers at Stanford and around the world, taking advantage of technological and processing improvements to advance the performance and minimize the cost of construction. The AWESOME receiver has now been verified through several years of testing and broad scientific usage. In this paper, we describe the AWESOME receiver, its components, design techniques, and then discuss its performance characteristics. A series of example observations illustrate the performance characteristics and their specific utilization in ELF/VLF experimentation.

II. Antenna Characteristics

The AWESOME receiver uses wire-loop antennas, each sensitive to the component of the magnetic field in the direction orthogonal to the plane of the loop. With two loops, whose planes are orthogonal both to each other and to the ground, it is possible to record the horizontal (i.e., along the Earth's surface) magnetic field at any location. Although it is also feasible to set up a third loop whose plane is parallel to the ground, for many applications this measurement is not as useful, since vertical magnetic fields are typically much smaller near the ground, except in the case of significant local subterranean inhomogeneities. The AWESOME receiver can also be configured to record a third signal from a vertical electric whip antenna, and although such a measurement is useful for certain specific applications, we focus in this paper only on the electronics and measurements taken with two orthogonal magnetic-loop antennas.

Choice in receiving antenna parameters is discussed by Paschal [12] and Harriman *et al.* [20] and are briefly reviewed in this paper. ELF/VLF magnetic-loop sensitivity and frequency response are controlled by four dependent antenna parameters: resistance (R_a), inductance (L_a), area (A_a), and number of turns (N_a). Sensitivity can be evaluated by comparing the antenna noise with the signal levels that would be induced from a certain magnetic field. Antenna noise is dominated by thermal noise of the wire resistance, given as

$$E_a = (4kTR_a)^{\frac{1}{2}} \tag{1}$$

in units of $\mathrm{V} \cdot \mathrm{Hz}^{-1/2}$, or noise spectral density, where k is Boltzmann's constant and T is absolute temperature in Kelvin. From Faraday's law of induction approximated when the wavelength is large as compared to the antenna size, the voltage induced in a wire loop from a magnetic field amplitude B at angular frequency ω is given as

$$V_a = j\omega N_a A_a B. \tag{2}$$

The above equation allows us to relate a given voltage level at the input of the receiver to an equivalent magnetic field value, since the N_a and A_a are characteristics of the antenna. This relation is an important property for calibration (discussed later), since the recorded values can therefore be converted to magnetic field values. Setting the noise level for a 1-Hz bandwidth in (1) to be equal to the voltage from a given magnetic field in (2), we can solve for the value of B to arrive at a field-equivalent and frequency-dependent signal level for E_a, written as

$$B_n = \frac{(4kTR_a)^{\frac{1}{2}}}{N_a A_a j\omega}. \tag{3}$$

The quantity B_n is a measure of the noise level intrinsic to the resistance of the antenna wire. We then normalize the result by $1/f$ to obtain a sensitivity metric

$$\hat{S}_a = \frac{(4kTR_a)^{\frac{1}{2}}}{2\pi N_a A_a} \tag{4}$$

in units of $\mathrm{T} \cdot \mathrm{Hz}^{1/2}$. The sensitivity as defined in this paper is simply the magnetic-field-equivalent value of the antenna's thermal noise in a 1-Hz bandwidth, normalized by the factor $1/f$.

The other important antenna parameter is the turnover frequency, $\omega_a = R_a/L_a$. For values of ω well above this frequency, the impedance of the antenna $(Z_a = R_a + j\omega L_a)$ is dominated by the inductance and is therefore proportional to ω. However, since the induced voltage in (2) is also proportional to ω, the current induced in the loop (V_a/Z_a) will remain essentially constant with respect to frequency. The result is a flat frequency response for the magnetic loop for frequencies well above ω_a.

As mentioned earlier, it is possible to improve $\hat{S}_a$ by simply increasing $(A_a M)^{-1/2}$, i.e., by increasing either the thickness of the wire, the area of the loop, or the number of turns. The antenna impedance also changes with these parameters, but for a specifically chosen antenna impedance (on the basis of the front-end impedance of the preamplifier), a family of different antenna parameters (with significantly varying values of $\hat{S}_a$) can satisfy the impedance requirements. Some examples of antenna parameters fitting the 1.00 Ω and 0.5–1.0-mH impedance are given in [20, Table 2].

Using (2), with values of $N_a = 5$ and $A_a = 25$ m^2, we see that a 1-pT amplitude signal at 10 kHz induces an electromotive force of only $\sim$7.8 μV in the wire loop, so that even the most sensitive loop is only useful if followed by low-noise amplification. Harriman *et al.* [20] describe the techniques for this amplification used in the AWESOME receiver, which consists of a transformer followed by a low-noise-amplifier circuit specifically designed for ELF/VLF signals. The transformer–amplifier pair involves balancing several tradeoffs, as described by Harriman *et al.* [20], but is generally capable of achieving, over $\sim$2 decades of frequency range, sufficiently low-noise figure so to add minimally (i.e., $<$ 10 dB) to the limiting antenna thermal noise and is designed specifically to match a given antenna impedance.

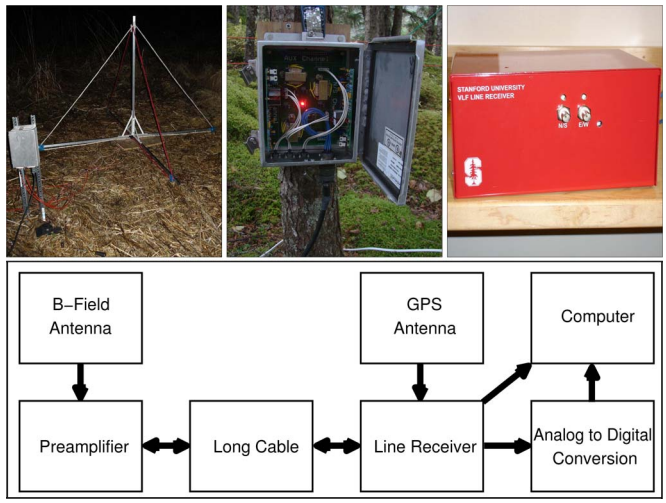

Fig. 1. Photographs and block diagram of the AWESOME receiver. (Top left panel) Pair of orthogonal wire loops, 1.69-m^2 area, mounted next to the preamplifier, pictured in Homer, Alaska. (Top center panel) Opened preamplifier box in operation in Juneau, Alaska. (Top right panel) Indoor line receiver box. (Bottom panel) Block diagram of the AWESOME receiver's main components, which reside outdoors (B-field antenna, preamplifier, long cable, GPS antenna) or indoors (line receiver, ADC, and computer).

III. System Design

We now describe the basic design principles of the AWESOME receiver. The top panels of Fig. 1 show photographs of the three main components of the AWESOME receiver: antenna, preamplifier, and line receiver. The AWESOME receiver samples data at 100 kHz, nominally facilitating signal detection up to 50 kHz without aliasing. Furthermore, the 16-bit sampling nominally enables 96 dB of dynamic range, although the practical dynamic range (discussed later) is a function of the input-referred system noise compared to the signal level which saturates or "clips" the receiver output.

In detecting magnetic field signals on the order of femtotesla to picotesla, a dominant source of interference is local electromagnetic fields from 50/60-Hz power lines, whose harmonics can extend to many kilohertz and whose strength can be orders of magnitude stronger than those of natural ELF/VLF signals. Some of the power-line interference can be tracked and subtracted in postprocessing, provided that the level of power-line interference has not saturated the output. However, it is nonetheless helpful to avoid this interference altogether by locating the loop antennas far away from such sources, whereas the recording computer must typically be placed indoors. Fig. 1, bottom panel, shows a block diagram showing how these goals are realized. The preamplifier, placed near the antenna, matches the impedance of the antenna and provides low-noise amplification. The preamplifier must be near to the antenna, as any long cable may contribute noticeable resistive losses as compared to the 1-Ω antenna resistance. At the output stage of the preamplifier, a variable-gain amplifier enables additional multiplication of the signal amplitude by either 0, 10, 20, or 30 dB. The proper choice of gain level is described later, since it affects both the noise characteristics of the receiver and its saturation level and may be different depending on application and choice of antenna.

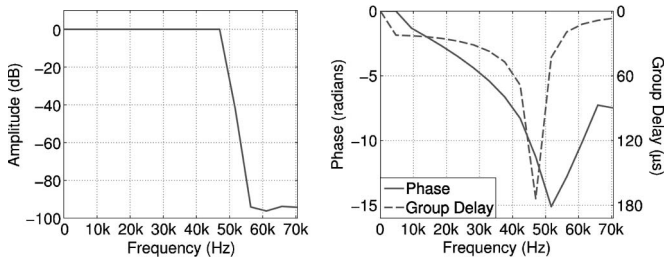

Fig. 2. Simulated performance of the 12th-order antialiasing filter utilized. (Left panel) Amplitude response, showing roll-off at 47 kHz, and ∼95-dB attenuation by ∼55 kHz, designed for 100-kHz sampling. (Right panel) Phase and group delay of the antialiasing filtering, showing a generally linear phase through ∼40 kHz.

The low-frequency response of the receiver (∼800-Hz cutoff) is limited mostly by the line transformer which matches the preamplifier with the transmission line. However, the low-frequency cutoff can be selected as 80 Hz, 350 Hz, 800 Hz, or 7 kHz. The first two are used for extremely quiet sites (i.e., located away from 50/60-Hz interference sources) and are achieved with a gain boost to the lower frequencies that roughly compensates the loss in frequency response below the turnover frequencies of the antenna and receiver, thus flattening the response at the low end. The third setting applies no frequency compensation. The 7-kHz high-pass filter is used at noisier sites, like rooftops of a building at a school or, in general, at urban sites, and generally in situations where only VLF transmitter signals in the 15–30-kHz range are of interest. The preamplifier also contains a passive radio-frequency-interference suppression circuit at the front consisting of a series inductor with shunt-to-ground capacitors at both antenna terminals to ensure that high-frequency (HF) RF sources [like AM radio stations or HF transmitters] do not couple in to the receiver. The total power usage of the AWESOME preamplifier is ∼1 W, or ∼33 mA of current from the ±15-V supply lines.

The line receiver, located indoors, performs antialiasing filtering, GPS time-stamping and synchronization, and passes both analog signal and sampling clock signal to a computer for digitization across a shielded cable. The line receiver also provides power to the preamplifier. Digitization is done with an internal PCI card in the computer, capable of up to three-channel 16-bit sampling at 100 kHz per channel. We currently utilize a card developed by National Instruments, like the 6250M, or a previous two-channel model, 6034E. The antialiasing filter is applied separately on each channel, using a 12th-order elliptical filter at 47 kHz. The filter reaches ∼95-dB attenuation by 55 kHz, as shown in the simulated amplitude and phase response in Fig. 2. Although the use of filter orders above eight is rare in practice, a 12th-order filter was employed in this paper in order to push the cutoff as close to 50 kHz as possible, so that VLF transmitter signals at 40.75 kHz (NAU, Puerto Rico) and 45.9 kHz (NSC, Italy) are within the passband of the receiver. The total power usage of the line receiver is ∼5 W.

A suitably long shielded multiconductor cable (currently Belden 1217B) connects the preamplifier to the line receiver and consists of four shielded 22 AWG twisted pairs, designated, respectively, to carry power from the line receiver to the preamplifier and up to three data channels from the preamplifier to the line receiver. For the three data channels, at both ends of the transmission line, a custom-designed line transformer matches the 75-Ω impedance to the output impedance of the preamplifier circuit and the input impedance of the line receiver (1.75 kΩ). Since the resistivity of the cable is rated as ∼5 Ω per 100 m and since the preamplifier regulates the ±15-V supply to ±10.8 V (and requires ±11.5-V minimum power voltage for supply-line regulation), the maximum cable length given the preamplifier's ∼1-W power is ∼2000 m. Typically, however, 150–500 m is sufficient to locate the antenna far away enough from power lines.

Since broadband data are sampled at 100 kHz, and 16 bits per sample, data will accumulate at ∼687 MB/h per antenna. Therefore, an entire 24-h data set on two orthogonal antennas will be ∼32 GB. To mitigate the large amount of storage required to capture all of this, custom data-acquisition software has been developed at Stanford. Broadband 100-kHz data can be saved for any desired daily schedule, in continuous fashion or in synoptic mode (i.e., periodic short snippets), the latter often being necessary due to the large volume (∼1.5 GB/h) of data. Narrowband data can be saved for as many as 16 channels (limited only by the processing power of the computer) and are typically saved in a single block for the whole day due the much smaller volume of data (∼15 MB/h). The software also enables selected amounts of data to be sent over the Internet to a server according to a daily schedule or transferred to another hard drive or storage medium for occasional collection. Live calibrated spectrograms can also be posted on the Internet. A so-called "pac-man mode" is sometimes used, which enables continuous data to be archived for several days backlog, with the oldest day being then deleted to make room for the newest day, to serve as a large buffer useful in the event of geomagnetic storms or other events in which the occurrence is not necessarily known until shortly thereafter. The data-acquisition software also includes a number of features intended to recover automatically and gracefully from a power failure or computer crash. For instance, the software automatically reboots the computer in the event of an interruption with the receiver signals or if the CPU is unable to keep up with the sampling process. Data are not currently being archived in a publicly accessible fashion, but such a system is currently being planned and will be described elsewhere.

IV. Calibration

Calibration enables the digitally recorded 16-b output of the AWESOME receiver system to be directly related to wave magnetic field values, although the frequency-varying gain of the receiver must be taken into account. This result is achieved via injection of a series of known-amplitude signals at the input of the preamplifier and measuring the values at the output. The corresponding value of the magnetic field is known through (2), since the parameters of the antenna, as well as the input impedance of the preamplifier, are known.

Although the calibration reference signal can be injected manually at the receiver input terminals (generally at a series of frequencies between dc and 50 kHz to span the whole receiver band), the AWESOME receiver includes an internal calibration

circuit which generates a pseudorandom digital sequence 1023 b long, with bit frequency of ∼256 kHz. In the frequency domain, this sequence corresponds to a comb of signals at frequency multiples of ∼250 Hz, with equal amplitudes at all frequencies below 50 kHz. Therefore, a single-calibration reference signal essentially includes all the frequencies to sample the amplitude response of the receiver with ∼250-Hz resolution, since the individual frequency components can be separately treated in postprocessing. This calibration technique has also been used in some earlier Stanford ELF/VLF receivers designed by E. W. Paschal.

By comparison of the calibration signal (separately at each frequency component) with the background noise level, we can also measure the noise levels intrinsic to the hardware of the receiver, including noise induced via its exposure to an electromagnetically noisy indoor environment (as electromagnetic noise may couple into the wires and circuit boards, particularly since shielding magnetic fields is generally not possible without the use of μ-metal material enclosures). Noise which enters the system through the antenna can be excluded, since the calibration signal can be recorded without an antenna attached to the preamplifier, using a "dummy loop" having the same impedance connected instead of the antenna. Furthermore, since the calibration signal corresponds to a specific magnetic field value for a given antenna [using (2)], the noise levels can be "input-referred" or related directly to a magnetic field spectral-density value, although a specific antenna configuration must then be assumed.

Although the pseudorandom calibration signal is incoherent, the phase response can be measured by injecting a signal from a sinusoidal source into one channel of the receiver and simultaneously into the other channel of the analog-to-digital converter (ADC). Since the ADC records one channel directly from the source and one channel from the source via the receiver, the phase difference in the recorded signal can be used to measure the delay in the signal and can be repeated manually for many frequencies. In practice, however, it is found that the phase response varies by a negligible amount between different AWESOME receivers, although the amplitude response may vary slightly (∼1 dB) due mostly to tolerances to the resistors used in the antialiasing filter. For this reason, an amplitude calibration is usually separately recorded for each receiver when it is placed in the field, whereas a generic phase calibration can be applied universally.

V. Gain and Sensitivity

We now describe some of the measured performance characteristics of the AWESOME receiver. Fig. 3 shows some measured properties of the AWESOME receiver. The top left panel shows the AWESOME receiver frequency response (in units of millivolts at the output divided by picotesla at the input). Although the measurement is made separately in both channels, only one is presented. In addition, these characteristics vary by a small amount between physical receivers, owing to tolerances in the various components. The 3-dB cutoff points are at ∼800 Hz (where the line transformer begins to attenuate the signal) and at 47 kHz (where the antialiasing-filter cutoff lies).

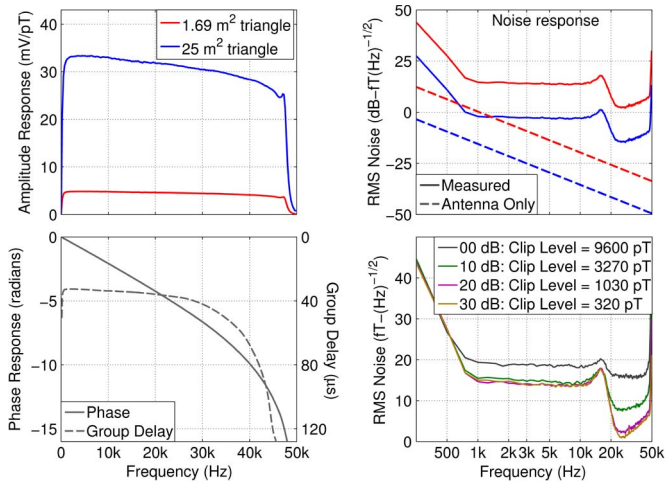

Fig. 3. Measured performance characteristics of the AWESOME receiver. (Top left panel) Amplitude response between 0 and 50 kHz, with calibration applied to convert to magnetic field units, for two different size antennas. The HF roll-off is dominated by the antialiasing filter, whereas the low-frequency roll-off (at about ∼800 Hz) is dominated by the transmission-line matching transformers. (Bottom left panel) Phase and group delay response for the receiver, although we note that the phase response is dominated by the impact of the antialiasing filter. (Top right panel) Noise performance of the antenna, for the same two sizes as in the amplitude response. The dashed lines show the input-referred noise which would result from the thermal noise of the 1-Ω antenna; the solid lines show the actual measured system performance, these data are shown at the 10-dB gain level. (Bottom right panel) For a fixed antenna size (same as the red curves in the upper plots), the noise level of the receiver as a function of the frequency. The clip levels are also calculated by determining the voltage at which the maximum ADC value is recorded.

In order to correspond the calibration-signal strength to an equivalent magnetic field, the size of the antenna must also be known. The frequency response is therefore presented for two different typical right-isosceles 1-Ω 0.5–1.0-mH antenna sizes: a large loop (25 m^2) consisting of a 10-m base and a 5-m height, and second being a smaller loop (1.69 m^2) with 2.6-m base and 1.3-m height. We refer to these two sizes (1.69 and 25 m^2) consistently throughout the description of the performance characteristics. It should be noted that although the calibration may vary slightly from receiver to receiver, the general characteristics described in this paper apply consistently across all measured AWESOME receivers.

The phase response, shown in the bottom left panel of Fig. 3, is obtained by injecting a sinusoidal signal into the front end of one of the receiver channels and also directly into the ADC as a reference. The derivative of the phase delay with respect to frequency gives the group delay of the receiver. Within the passband (i.e., between 1 and 45 kHz), the group delay is mostly between 25 and 35 μs (or approximately three samples at 10 kHz), rising above 50 μs above 40 kHz as the frequency nears the 47-kHz cutoff of the antialiasing filter.

The top right plot of Fig. 3 shows the measured input-referred rms noise levels with solid lines, for the same two antenna sizes as in the top left panel. The theoretical noise level of a noise-free receiver (where only thermal noise from the 1-Ω 0.5–1.0-mH antenna is present) is shown with dashed lines. The vertical separation between solid and dashed lines is therefore a measure of the noise added in the receiver electronics. We note that the noise measurements are taken when the receiver is deployed in the field, as opposed to inside a μ-metal shielding

chamber, so all effects of environmental noise coupling into electronics are inherently included. This particular noise response is shown for the 10-dB preamplifier gain setting.

We may use this noise floor to establish the minimum detectable signal (i.e., the smallest signal for which signal-to-noise ratio (SNR) is 0 dB), which is a function of the bandwidth of the signal being detected (since the total noise power depends on the bandwidth or, alternatively, on the integration time used in signal detection, which intrinsically sets the bandwidth). VLF transmitter signals operate over a $\pm$100-Hz bandwidth, in the frequency range between 18 and 30 kHz, where the receiver noise levels are ~ -10 dB $\cdot$ fT/Hz$^{1/2}$ amplitudes for the large antenna configuration, as shown in Fig. 3, top right panel. Hence, the 200-Hz bandwidth includes total receiver noise of $\sim +13$ dB $\cdot$ fT, indicating that VLF transmitter signals in this configuration as low as $\sim$4–5 fT can be received with 200-Hz time resolution. Similarly, sensitivity over the ELF frequency range enables detection of signals over a 1-Hz bandwidth (i.e., for signals of longer duration such as chorus needing only 1-s time resolution) as low as $\sim$1 fT with the larger (25 m^2) antenna configuration.

The natural ELF/VLF radio environment on the Earth is dominated by the presence of so-called radio atmospherics [19], or "sferics," impulsive ($\sim$1 ms) broadband radiation originating from lightning strokes even at global distances from a given receiver. Typical sferic amplitudes at distances greater than 500 km are 1–100 pT. Other natural sources of ELF/VLF radiation detected on the ground such as chorus [21], hiss [22], and whistlers [7] are often present with substantially smaller amplitudes ($<$ 1 pT). The root-mean-square average spectral density of natural ELF/VLF noise is typically between 1–100 fT/$\sqrt{\text{Hz}}$ in this frequency range [19]. Signals can also be generated artificially via HF (3–10 MHz) heating of the auroral lower ionosphere, with amplitudes as strong as several picoteslas [23] or greater. The AWESOME receiver is sensitive enough to detect even weakly present natural ELF/VLF signals.

The choice of gain settings may affect the noise performance of the receiver, at the expense of "clip level," or the lowest amplitude signal which may cause saturation of the receiver output, which in turn affects the dynamic range. Fig. 3, bottom right panel, shows the input-referred noise response for the receiver (with the 1.69-m^2 triangle antenna) using all four preamplifier gain settings. Since a higher gain may cause the noise levels generated in the preamplifier to be higher than the noise levels generated in the line receiver, increasing the gain from 0 to 10 dB lowers the input-referred noise response of the receiver (although increasing beyond 10 dB shows only marginal improvements). On the other hand, increasing the gain decreases the threshold clip level. The effective dynamic range can be taken to be between the receiver noise level and the clip level. For instance, using the 0-dB preamplifier gain setting with the larger (25 m^2) antenna configuration, the total noise level (i.e., the input-referred field spectral density integrated over the bandwidth) in the passband of the receiver (i.e., between 1 and 47 kHz) is $\sim$1.6 pT, or $\sim$75 dB (12.5 b) below the clip level. At 10-dB gain setting, the broadband dynamic range is $\sim$71 dB, while at 20-dB gain, the dynamic range is $\sim$62 dB, and at 30-dB gain, the dynamic range is $\sim$53 dB. Hence, while increasing the gain enables smaller signals to be detected, such a result comes at the expense of the ability to fully record the largest signals without incurring receiver saturation. For this reason, the 20- and 30-dB gain settings will likely only be used in situations where only small signals are of interest, since the high gain will reduce the effect of quantization noise, at the expense of dynamic range.

VI. Timing Accuracy

An accurate 100-kHz sampling clock is crucial for phase-coherent measurements of VLF transmitters and to maintain the possible use of VLF interferometry involving coherent measurements between sites. For instance, a clock drift of even 1 μs (one tenth of a sample period at 100 kHz) represents 9° of phase uncertainty at 25 kHz, while ionospheric disturbances often occur with phase changes on the order of 1° or less [24]. GPS devices often provide a 1-pulse-per-second (PPS) timing signal, from which the 100-kHz sampling signal must be derived. The GPS timing card used in the AWESOME line receiver (Motorola M12M OnCore) guarantees 10–20-ns absolute timing on its 1-PPS clock, but in order to extend this timing accuracy to the 100-kHz sampling signal, the AWESOME receiver uses a feedback scheme consisting of a 10-MHz voltage adjustable oscillator, whose control voltage is set by a complex programmable logic device (CPLD) via a 10-bit digital-to-analog converter (DAC). The CPLD counts 10-MHz cycles between each 1-PPS GPS pulse and adjusts the 10-MHz oscillator speed accordingly. The 10-MHz clock is then divided down to obtain the 100-kHz sampling clock; therefore, maintaining an exact frequency of the 10-MHz clock drives the generation of an accurate 100-kHz sampling clock. Without the use of a feedback system, the 10-MHz clock is guaranteed accurate to 1 ppm (i.e., 1 μs). A block diagram of the feedback scheme which improves this accuracy by a factor of 10–100 is shown in the top panel of Fig. 4.

At the start of each second, the 100-kHz clock is reset to force a rising edge, but the absolute timing may nominally drift over the course of the second, depending on the frequency error of the 10-MHz clock. In principle, the timing accuracy of such a system should be at least within one period of the 10-MHz clock (i.e., 100 ns or 0.1 ppm), since the CPLD can adjust the 10-MHz clock based on the integer number of cycles between each 1-PPS signal. However, even an error of a fractional number of samples per second of the 10-MHz clock would eventually cause it to overshoot or undershoot the number of counts within each second, so better than 100-ns accuracy should, in general, be achievable. Because the 10-b DAC (i.e., 1024 states) adjusts the speed of the 10-MHz clock over a $\pm$5-parts-per-million range, an accuracy as good as $\sim$0.01 parts per million (or 10 ns) may be achievable with this feedback system, if appropriate oscillator-adjustment schemes are chosen. By design, the timing feedback keeps the 10-MHz clock slightly slower than ideal, but the feedback scheme is designed to keep this margin as small as possible.

This drift present in practice can be quantified by monitoring the phases of VLF transmitter signals, which use extremely stable oscillators to maintain a consistent frequency for

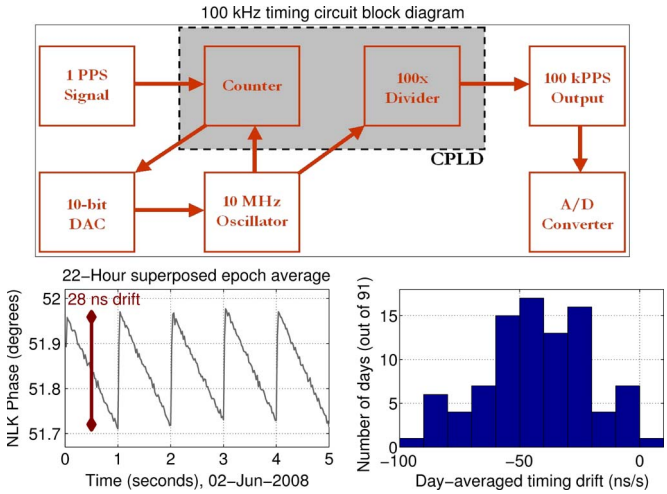

Fig. 4. (Top panel) Basic operation of an internal circuit designed to produce a 100-kHz GPS-synchronized sampling clock. A 1-PPS signal is provided by a GPS module, which is used to synchronize the system. A CPLD device counts cycles from a 10-MHz adjustable oscillator and adjusts the clock frequency via a 10-bit DAC if the number of 10-MHz clock counts during the second is either too many or too few. The 10 MHz is then divided down by 100× to generate the 100-kPPS sampling clock. (Bottom left panel) Phase of the NLK transmitter, tracked with 50-Hz time resolution and superposed so that consecutive 5-s blocks over a 23-h period are summed into an average 5-s epoch. The drifting phase indicates that a 28-ns timing offset occurs within each second, which is subsequently corrected at the beginning of each second. The NLK transmitter has highly accurate frequency standard, essentially acting as a timing reference (after proper demodulation of the MSK signal). (Bottom right panel) Twenty-three-hour superposed epoch process repeated for 91 days in the Summer of 2007, for a receiver at Stanford University. The average drift typically lies between −20 and −60 ns/s, indicating that the absolute accuracy of the timing signal to be no worse than the 100 ns typically afforded by GPS.

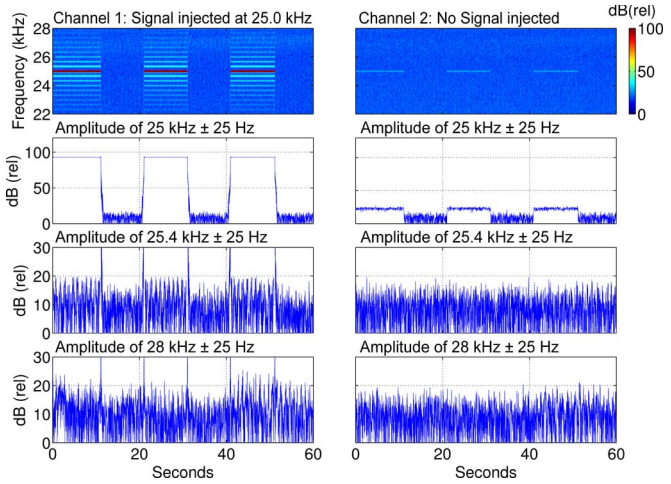

Fig. 5. Left and right columns correspond to channels 1 and 2 (respectively) of an AWESOME receiver, recorded with a strong signal manually injected into channel 1 at 25 kHz. The top spectrum shows the signal in channel 1, while a substantially weaker (∼70 dB) signal is cross modulated onto the other channel. The second row shows a narrowband extraction around 25 kHz, where the cross-modulated signal onto channel 2 can be observed to be present, but strongly attenuated. The third and fourth rows show the same narrowband amplitude extractions for frequencies of 25.4 and 28 kHz that little or no 25-kHz signal is observed at frequencies other than 25 kHz. A small modulation is visible in the 25.4-kHz panel on channel 1, but this is due to signal-processing limitations of the window used, not actual nonlinear cross modulation in the receiver.

broadcast. These transmitter signals are typically modulated with a minimum shift keying (MSK) 200-Bd communication scheme over a 200-Hz band. Software written at Stanford University for use with the AWESOME (described later) is used for demodulating the MSK-related frequency variations, thereby obtaining an effective continuous-wave (CW) signal with a known phase as compared to GPS. Therefore, timing errors are reflected as a systematic drift in the recorded phase of these signals over the course of each second.

To detect this systematic drift, a number of consecutive periods of data can be summed up, i.e., an average epoch can be calculated by superimposing many epochs on top of each other. The bottom right panel of Fig. 4 shows a 5-s superposed epoch analysis of 23 h of phase data from the NLK transmitter in Jim Creek, WA, operating at one of two frequencies at 24.85 and 24.95 kHz and recorded at Stanford on June 2, 2008 (part of the same data set shown in the lower left panel of Fig. 7). This result therefore represents the average of 16 560 repetitions of the 5-s cycle, which makes any systematic recurrent drift evident above the general noise levels by effectively removing all variations that are not periodic at 0.2 Hz. The saw-tooth variations of 1-s period clearly visible are the phase errors generated by the residual imperfection of the AWESOME's sampling clock, with the corrections occurring at the start of each second with synchronization of the sampling clock with GPS. In this case, the phase drift is $\sim 0.2^\circ$ at 24.8 kHz, corresponding to a timing error of ∼28 ns or an accuracy of 0.028 parts per million of the 100-kHz sampling clock. The same test was repeated for 91 days from April through July 2008 when both the NLK transmitter and AWESOME ELF/VLF receiver operated continuously, and the distribution of these day-averaged errors are shown in the lower right panel of Fig. 4. Of the 91 days, 81% showed phase drifts below 60 ns, and none showed a phase drift above 100 ns. The averaged timing drift is ∼40 ns. These results are consistent with a systematic timing drift time-varying between 0 and 100 ns/s. Additional improvement in the timing accuracy can be achieved by increasing the speed of the 10-MHz clock.

VII. Cross Modulation and Cross Coupling

In addition to the need for highly phase-coherent sampling, a number of VLF experimental measurements rely on ionospheric modifications induced (either directly or indirectly) by a VLF transmitter, which affect the propagation of a second VLF transmitter path through the disturbed region [25]. Thus, an ON–OFF signal imposed onto the first source may also be imposed in the secondary source via this nonlinear coupling in the ionosphere. Examples of this are transmitter-induced precipitating electron radiation [26] and radio-wave ionospheric heating from VLF transmitters [25], [27] and HF antenna arrays [28], [29]. However, such experiments can be complicated by the possibility of cross modulation in the receiver if the degree of possible cross modulation in the receiver is not properly quantified [25], [30]. In addition, cross coupling between two channels in the receiver can also affect these experiments and may also adversely affect magnetic direction finding using the two channels, such as what is done with radio atmospherics from lightning [31].

Fig. 5 shows the results of a test to characterize both the cross-modulation and cross-coupling effects. A 25-kHz signal

is injected into one of the receiver channels, while the second channel is left with no signal. The top panels of Fig. 5 show the spectrum of both channels, with the 25-kHz input signal clearly visible in the top left panel. We note that the sidebands of the 25-kHz signal are a product of the spectrogram windowing and are not really present in the receiver output. The top right panel shows that the injected signal does indeed cross couple between the two channels but at a recorded signal level that is $\sim$70 dB smaller than the original signal, the rest due to a small amount of coupling, perhaps from the grounding or shared power-supply sources between the two channels. The second two panels in Fig. 5 show a narrowband filter applied around 25 kHz, with a $\pm$25-Hz band, in order to extract the amplitudes of both the directly injected signal as well as the cross-coupled signal. The lower four panels of Fig. 5 show identical narrowband filter but applied at frequencies that are 400 Hz and 3 kHz higher than the 25-kHz input signal. As the third pair of panels show, a small cross-modulation effect is shown in the same channel as the injected signal at a frequency of 25.4 kHz, but this detected signal is again $\sim$70 dB smaller than the 25-kHz signal itself and is actually due to the imperfections of the digital finite-impulse-response filter applied. There is no cross modulation on the other channel, and furthermore, there is no detectable cross modulation (within at least 80 dB of the input signal) on either of the two channels at 28 kHz. Although not shown, similar tests at other frequencies yielded very similar results. The result implies that there will be no receiver-induced cross modulation between two strong signals, particularly if one of those strong signals undergoes amplitude modulation, as in the case of VLF transmitter keying [26].

VIII. Sample Data

We now proceed to show some sample data taken with the AWESOME receiver. Fig. 6, top panel, shows a 1-min segment of data, recorded at Chistochina, Alaska (at 62°37′ N, $-144°37'$ W). Only data from one of the two operating antennas are shown. ELF/VLF data recorded at this particular location are exceptionally free of electromagnetic interference due to the remoteness of the location (i.e., away from cities and strong power lines) and the long cable between antenna and computer ($\sim$500 m at the time of this recording). The top panel shows the data in spectrogram form, i.e., the data are divided into overlapping discrete time bins, with a short-time Fourier transform then performed on each time bin, between 0 and 50 kHz. The amplitude of received signals in each frequency bin, and for each time bin, is indicated with the color bar. In the top spectrogram, we divide the data into 10-ms bins, so that the ΔF frequency resolution is 100 Hz. In the bottom spectrogram, the data bin size is 50 ms (i.e., $\Delta F = 20$ Hz). Longer bins have less bandwidth within each bin, and therefore less noise, although the time resolution is correspondingly reduced.

The horizontal lines in the top panel between 18 and 28 kHz correspond to VLF transmitter signals operating for long-range communication with submerged submarines. The pulsed lines between 11 and 15 kHz originate from a set of three transmitters across Russia known as the Alpha network.

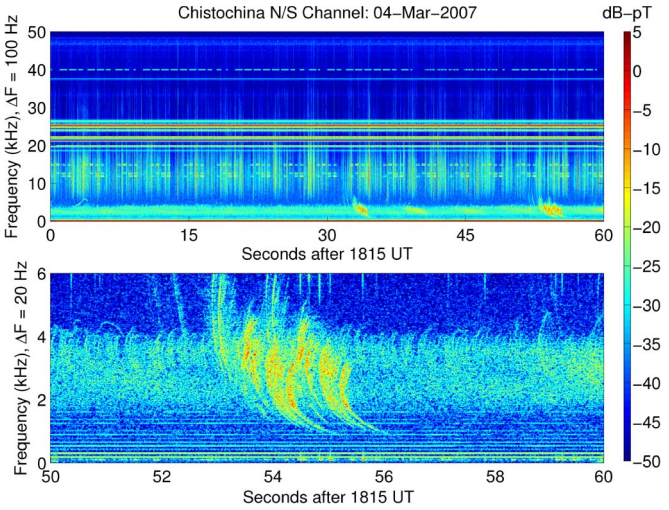

Fig. 6. Sample ELF/VLF data taken with the AWESOME receiver at Chistochina, Alaska. The top panel shows 60 s of data, with frequency on the y-axis, and the color bar indicating the strength of the magnetic field. The spectrogram divides the data into short pieces (in this case, 100 pieces per second) and applies a short-time Fourier transform to each segment. The thin vertical lines correspond to radio atmospherics, short bits of impulsive radiation, originating at lightning strokes, which can be at global distances from the receiver and guided by the Earth-ionosphere waveguide. The horizontal lines between 20 and 30 kHz correspond to constant MSK-modulated VLF transmitters operated by various national navies for long-distance communication with submarines. The pulsed signals between 10 and 15 kHz correspond to the so-called Alpha navigation system, a set of three VLF transmitters operated by Russia. The bottom panel shows a zoom-in of the lowest frequencies and the last 10 s of the record, where a "whistler" can be clearly observed. Whistlers originate from lightning, but the energy escapes in the atmosphere and propagates in the so-called whistler mode along ducts, or guided paths along magnetic field lines, where they can undergo dispersion and arrive at the opposite hemisphere. In these records, all natural and man-made phenomena are clearly received with very high SNR and time resolution.

These transmitters, each of which alternate between three different frequencies, using 400-ms pulses and a 3.6-s cycle time, serve as a navigation beacon via amplitude and phase triangulation of the signal from the three transmitters and are analogous in principle to the "Omega" transmitters [5]. A particular experiment involving these Alpha signals is discussed later.

The thin vertical lines in the spectrogram are so-called radio atmospherics, or sferics, which originate from lightning strikes at global distances. Although these sferics propagate efficiently in the Earth-ionosphere waveguide at VLF frequencies, a portion of the propagating signal leaks upward through the ionosphere, entering the magnetosphere in the form of a whistler-mode plasma wave. In the presence of field-aligned electron-density structures in the magnetosphere known as ducts, these "whistlers" can be guided to the geomagnetic conjugate point, exhibiting strong dispersion due to frequency-dependent propagation speeds well below c, although the availability of ducts is a strong function of magnetospheric and geomagnetic conditions. The phenomenology of whistlers is described in detail in [7]. The bottom panel of Fig. 6 shows a close-up of one of these received whistlers, where a number of discrete frequency-time traces are visible, possibly corresponding to multiple available ducts in different places, each guiding the VLF radiation from the same lightning source. The whistler is also surrounded by a band of energy between 2 and 4 kHz,

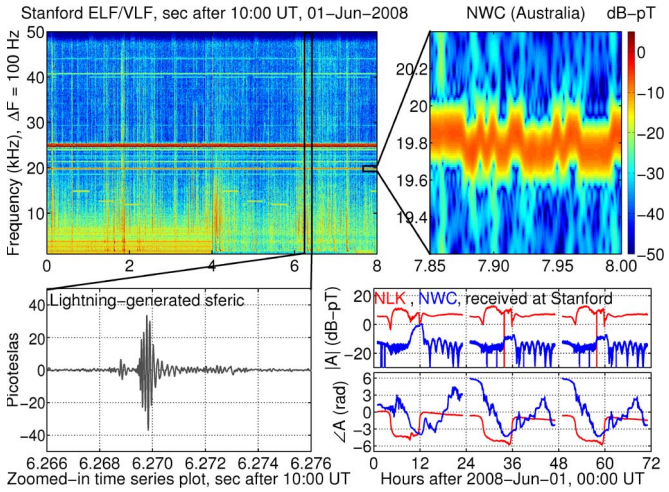

Fig. 7. Sample AWESOME data taken near Stanford University. (Top left panel) ELF/VLF spectrogram, in the same format as the top panel of Fig. 6. The first four seconds of the data are unprocessed, the second four seconds are shown after application of a postprocessing filter to remove the presence of coupled power-line energy at multiples of 60 Hz. (Top right panel) Close-up of a VLF transmitter signal broadcast from Northwest Australia, known as NWC, at 19.8 kHz. The 200-Bd modulation (5-ms bit periods) can be seen in the spectrogram. (Bottom left panel) Close-up of a radio atmospheric, lasting ∼1 ms. (Bottom right panel) Amplitude (top) and demodulated phase (bottom) of the NWC and NLK transmitters, received at Stanford University over a 3-day period. The diurnal pattern occurs due to day/night changes in the ionosphere.

known as plasmaspheric hiss, a form of natural noise present in the radiation belts, sometimes formed by repeated injection of energy from lightning strikes into these ducts.

Fig. 7 shows sample data taken at a site near Stanford University, electromagnetically quiet enough for VLF recordings although not as quiet as Chistochina. The antenna used is also slightly smaller and less sensitive than that at Chistochina. As shown in the first 4 s of the top left panel, the data below ∼5 kHz are affected by harmonics of ∼60 Hz coupled from power lines, so-called "hum." In this particular case, we have applied a technique to the second half of this record in order to mitigate the hum. The time-varying fundamental frequency of the power-line fields is first calculated, and the data are then convolved with an exponentially decreasing pulse train spaced out by the time-varying fundamental period. The resulting signal consists only of the frequency components at harmonic multiples of the fundamental frequency, and this result is then subtracted from the original data. This technique can be used to substantially reduce the hum visible in the spectrogram, with minimal change to the frequency content of real signals like radio atmospherics. An example of a radio atmospheric is shown in the bottom left panel of Fig. 7, exhibiting a duration and shape that is dependent on the characteristics of the lightning and the specifics of the propagation in the Earth-ionosphere waveguide [32].

A number of VLF transmitters are also detectable in the frequency range between 19 and 26 kHz, as shown in the top left panel of Fig. 7. These transmitters typically communicate with MSK modulation, in which the frequency takes on one of two values, representing a binary signal. Many transmitters operate with 200 Bd, i.e., bit durations of 5 ms, and a ±50-Hz frequency shift but covering ± ∼100 Hz of spectrum from the nominal center frequency. The top right panel shows a zoom-in of the transmitter signal from NWC, operating at 19.8 kHz and located in North West Cape, Australia (21° 48.96′ S, 116° 9.96′ E), and received at Stanford University. The MSK pattern can be clearly seen as frequency variations in 5-ms increments.

The amplitude and phase of these VLF transmitters received at a certain location are indicators of ionospheric changes and have been used to remotely sense a wide variety of geophysical phenomena. The bottom right panels of Fig. 7 show the amplitude (above) and phase (below) of the NLK transmitter in Washington State, U.S. (operating at 24.8 kHz) in red (48° 12.18′ N, 121° 55.02′ W), and the NWC transmitter in blue, recorded over a 72-h period at Stanford University (37° 4′ N, 122° 15′ W). We note that the NLK transmitter is much closer to Stanford (∼1.2 Mm) than the NWC transmitter (∼14.4 Mm) and is nearly directly north from Stanford, whereas the NWC–Stanford path is significantly east–west. Despite the very large distance from Stanford (more than 1/3 the circumference of the Earth), the NWC transmitter signal is clearly and unambiguously detected during the entire period, with signal amplitudes nearly always remaining > 20 dB above the ∼4–5-fT detection threshold. Both transmitter signals also show a clear diurnal pattern, with signal amplitudes that are higher during the ionospheric nighttime, when attenuation is smaller [2, p. 387]. However, the long east–west component of the NWC–Stanford path means that there is a relatively short period during which the path is entirely night, around 12 UT of each day. The periodic peaks and nulls that follow this period occur as a result of the sunrise terminator moving across the Pacific Ocean between Stanford and Australia, causing mode conversion to occur at the terminator [33]. The phase also shows a clear diurnal pattern and an advance in the phase (due to a lowering of the ionospheric reflection height) as the nighttime ionospheric path turns into a daytime one.

IX. Applications

We now describe a number of particularly useful applications of ELF/VLF data taken from the AWESOME receiver, in the context of geophysical studies of the ionosphere and magnetosphere. A number of other potential applications (such as imaging of underground structures, geophysical prospecting) are not covered in this paper.

A. Radio Atmospherics

The natural radio noise in the ELF/VLF range is dominated by impulsive radiation from lightning strokes known as sferics [19]. The global lightning rate is estimated to be ∼40/s but with strong diurnal, seasonal, and geographic variations [34]. However, since lightning events often consist of multiple strokes [1, p. 10] and since these sferics can be detected at global distances, or even multiple times from the same stroke, the sferic rate at a given receiver can be as high as hundreds per second.

Data from the AWESOME receiver can be very useful to study the properties of lightning that generates these sferics, the global occurrence of lightning, as well as the ionosphere along the propagation path. Fig. 8 shows the correspondence

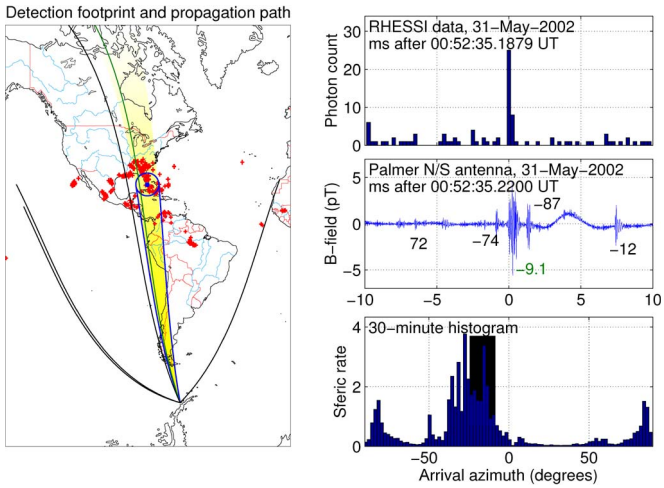

Fig. 8. Figure adapted from [35]. Using ELF/VLF data for studies of TGFs. The map on the left shows the location of the RHESSI spacecraft on May 31, 2002, indicated with a blue dot and circle, in the Caribbean. The red dots show LIS-detected lightning strokes, which indicate that a thunderstorm was also present in the area. (Top right panel) Gamma ray counts detected by RHESSI, indicating a short TGF. (Center right panel) Stanford ELF/VLF data taken from Palmer Station, Antarctica, over the same 10-ms period. After adjustment for speed-of-light propagation delays, a sferic, originating from a lightning stroke, is clearly detected, and its calculated arrival azimuth (indicated by the green text label in the plot and the green line in the map) is consistent with its arrival from the region underneath RHESSI. The other sferics in the record (whose arrival azimuths are shown in black text and also indicated on the map) do not appear to be coming from this region, however (indicated with blue lines in the map). (Bottom right panel) All sferics over a 30-min period are sorted by arrival azimuth and plotted. The highlighted portion (black on the histogram, yellow on the map) indicates the range of azimuths corresponding to the region underneath RHESSI. Elevated sferic activity is consistent with the presence of lightning activity underneath RHESSI.

between a so-called terrestrial gamma-ray flash (TGF) and a radio atmospheric detected at Palmer Station, Antarctica, as was reported by Inan *et al.* [35]. TGFs are short ($\sim$1 ms) bursts of gamma-rays discovered first by the Compton Gamma Ray Observatory [36] and later by the RHESSI spacecraft [37] and are presumed to be originating from bremsstrahlung from energetic electrons up to 35 MeV and occurring within a few milliseconds from lightning strokes [38], [39].

The left panel of Fig. 8 shows data from the Lightning Imaging Sensor (LIS) spacecraft indicated in red, whereas the blue dot and circle show the location of the RHESSI spacecraft, between Cuba and Florida, when a TGF event was detected on May 31, 2002, as was also reported by [35]. The RHESSI photon data are shown in the top right plot. The ELF/VLF waveform at Palmer Station, Antarctica (after accounting for the propagation delay to $\sim$10 Mm) shows a clearly defined sferic within $\sim$1 ms of the expected time of arrival (in this case, shown at $t = 0$), as is shown in the right center panel. Since the sferic is separately recorded on both the north–south and east–west antenna, the sferic can be determined to have arrived from a certain direction with $\sim 1^\circ$ accuracy [31]. In addition, the sferic indicated (with green) was the only one arriving from the region of RHESSI within the $\pm$10-ms window, whereas the others (labeled in black) are determined to have arrived from different directions.

Furthermore, the large number of sferics enables phenomenology of storms even from a single site. In the bottom right panel, a histogram of all sferics received over a 30-min period around the TGF time is sorted by arrival azimuth. The specific direction toward the RHESSI spacecraft exhibited a very large number of sferics, consistent with the presence of a strong thunderstorm in that area. With multiple sites, it is possible to determine the locations of individual sferics via time or arrival and direction-finding triangulation [40].

B. *Ionospheric Remote Sensing*

Ionospheric disturbances affect the propagation of the VLF transmitter signals described earlier, changing their received amplitudes/phases at a given receiver. These ionospheric disturbances are now known to be associated with an extremely broad array of geophysical phenomenon, including direct heating from lightning [41], electron precipitation induced by lightning [42], auroral precipitation [43], sprites [44], solar flares [45], geomagnetic storms [46], earthquakes [47], magnetars [48], solar eclipses [49], and gamma-ray bursts [50]. The associated VLF perturbations therefore lead to insight on the physical processes as well as their impact on the ionosphere.

While recording the amplitude of the transmitter signal is straightforward, measuring the phase requires detecting and removing the MSK modulation pattern so that the VLF transmitter signal can be treated as if it were a CW transmission. The recording software currently utilized enables this phase-demodulation process on a large number of VLF transmitter channels simultaneously, with the amplitude and phase extracted in real time. The time resolution of these data is typically 20 ms, fast enough to capture the temporal development of VLF perturbations. A basic approach to this MSK demodulation is described by Paschal [16], but the details of the algorithm for extraction of the MSK-demodulated phase will be described elsewhere.

Two examples of the detection of direct-coupled ionospheric disturbances induced by lightning (occurring just 5.6 s apart), or so-called Early–fast events, are shown in Fig. 9. The top left panels show the two radio atmospherics which generated these so-called Early/fast VLF event. These events are detected on the NML transmitter at 25.2 kHz from LaMoure, North Dakota, and received at Taylor, Indiana. The transmitter signal over a 0.4-s period for each case is shown in the top right panels of Fig. 9, which correspond to the times of the two radio atmospherics in the top left panels. Although the radio atmospheric is brief (appearing only as a thin vertical line in the spectrogram), the change in the transmitter-signal strength is immediately apparent and persistent. The bottom left panel shows the NML transmitter signal over a longer segment of time (to include both events), where the complete recovery (on the order of tens to hundreds of seconds [51]) can be observed separately for both events. The $\sim$2-dB perturbation is clearly stronger than the typical noise variations that existed during this period. Furthermore, the perturbation can also be detected in the phase plot, with the phase of the NML changing by $\sim 12^\circ$ for the first perturbing event. However, no significant phase anomaly is present for the second ionospheric disturbance, which is likely a consequence of the changing ionospheric conditions induced by the earlier lightning stroke.

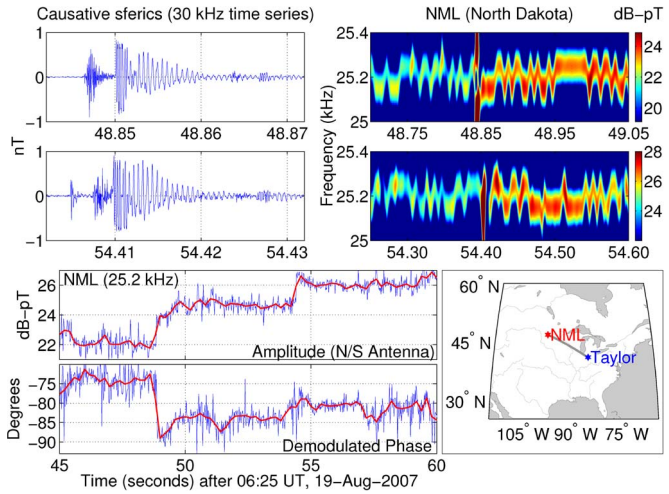

Fig. 9. Detection of direct-coupled ionospheric disturbances induced by lightning, so-called Early–fast events. (Top left panels) Two large sferics, ∼5.6 s apart, are detected at a receiver in Upland, Indiana. (Top right panels) Amplitude of the NML transmitter, at 25.2 kHz, during a 50-ms period around the sferic. The sferic itself appears as a brief vertical line in the spectrum, due to its impulsive nature. However, the NML transmitter signals strengthen by a few decibels after each of these sferics. The amplitude and phase of NML over a longer (15 min) period is shown in the two bottom left panels, indicating abrupt changes in the amplitude and phase, followed by a recovery which takes several minutes. The bottom right map shows the location of the NML transmitter and the receiver at Taylor University, from which it can be inferred that the ionospheric disturbance occurred somewhere along the great circle path. Although not shown, other transmitter signals (which arrive from different directions) do not show the abrupt change that is evident in the NML signal.

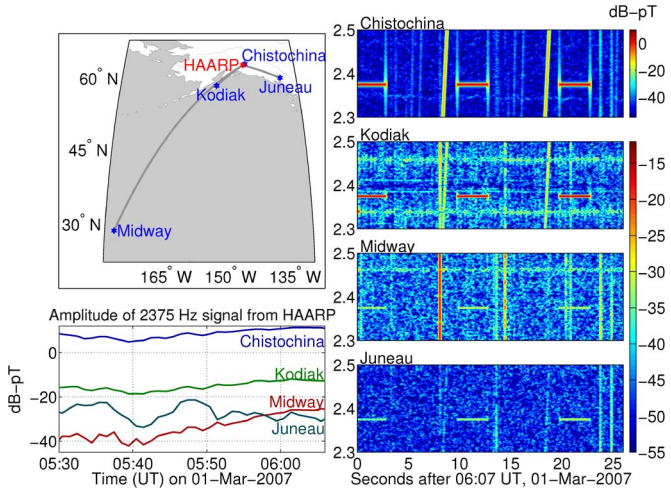

Fig. 10. Global detection of an ELF/VLF signal generated from an ionospheric heater. (Top left panel) Map showing the HAARP facility in red (in Alaska), and the locations of four receivers in Alaska and the Pacific Ocean. (Right panels) Spectrogram of the signal received at all four sites, on March 1, 2007. In this case, the transmitted format included 3-s long tones at 2375 Hz, which are clearly detected in the spectrogram at all four sites (i.e., with integration times in the 100-ms range). (Bottom left panel) Signal amplitude tracked at all four receivers over a 37-min period, showing some independence of the variation due to changing ionospheric conditions along the path or changing ionosphere or electrojet conditions above HAARP.

Early/fast events are associated in many cases with sprites [52], which occur through heating and ionization of the D-region in association with a powerful lightning stroke, and some Early/fast events may also be connected to in-cloud lightning activity [53].

Although not shown, we note that no similar perturbation was found on any other VLF transmitter signals detected at Taylor, indicating that the ionospheric disturbance is likely localized spatially. A closely spaced array of such receivers in the Western U.S. has been used to deduce the area of lightning-associated ionospheric disturbances [54].

C. ELF/VLF Generation and Detection

VLF transmitter signals typically operate in the 18–30-kHz range, as such frequencies can be generated by a tall vertical dipole, and can propagate with very low attenuation (a few decibels per megameter) in the Earth-ionosphere waveguide. In addition, the deep penetration into conductive seawater due to the skin effect enables communications with submerged submarines. However, generation of signals below ∼10 kHz (where even deeper penetration into seawater occurs) becomes increasingly less efficient given the practical constraints of using a sufficiently tall vertical dipole. Unfortunately, a long horizontal dipole is also inefficient because of its close proximity to the conducting ground beneath it. For instance, the ELF facilities located in Wisconsin and Michigan used grounded horizontal wire to operate at 76 Hz, but even with a length of about 150 km, these sites managed to radiate only ∼10 W [55].

For this reason, ELF/VLF generation via modulated heating of natural ionospheric currents [56], [57] has been investigated as a possible means of ELF/VLF communications [58]. The High-frequency Active Auroral Research Program (HAARP) facility located near Gakona, Alaska (62.39° N, 145.15° W), uses 3.6 MW of HF (2.7–10 MHz) power in a phased-array configuration to heat the ionosphere with a focused beam (∼5°–30° width), thereby changing the ionospheric conductivity. By modulation of this heating in the presence of the auroral electrojet (so that the electrons are heated and then cool periodically), the periodic conductivity changes turn the lower ionosphere into a large radiating antenna, whose generated signals can be detected across Alaska [23] and at distances at least 4400 km [59]. A technique known as geometric modulation generates stronger signals (7–11 dB), and an ELF/VLF phased array, via motion of the HF beam and no modulation of the power [60].

Fig. 10, top left panel, shows the placement of AWESOME receivers for detection of subionospherically propagating VLF signals generated above the HAARP facility using AM-modulated HF heating, at three different sites in Alaska: Chistochina (62.61° N, 144.62° W, 37 km from HAARP), Juneau (58.59° N, 134.90° W, 704 km SE of HAARP), and Kodiak (57.87° N, 152.88° W, 661 km SW of HAARP). Each of the Alaska sites use large 1-Ω antennas 18 m^2 in area or larger. Midway Atoll is located at 21.21° N, 177.38° W, 4466 km SE of HAARP, where a substantially smaller 1.7-m^2 antenna is used. The lower left hand panel show the detected 2375-Hz signals from HAARP for each of the four sites on March 1, 2007, during a 37-min period when the transmission format was consistent and the signal generation process in the ionosphere was particularly effective.

Moore *et al.* [59] integrated ELF/VLF data for 60 min at Midway in order to detect signal levels from HAARP at ~ -55 dB · pT, the farthest such unambiguous detection of ELF signals generated via this technique. However, in 2007,

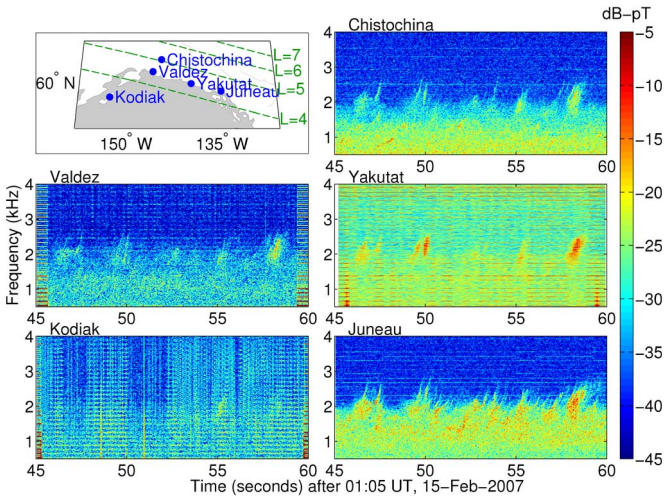

Fig. 11. Multistation simultaneous chorus emissions detected in Alaska, as presented by [21]. (Top left panel) Map showing the location of five receivers, over a range of L-shells between ∼3.5 and ∼5.0 and also a span of longitudes. The remaining panels show the same chorus elements detected at all five sites, over a 15-s period, although the emissions are detected most strongly at Juneau and Yakutat and weakest at Kodiak. The Yakutat receiver uses a smaller less-sensitive antenna and, therefore, has elevated noise levels. The data from all but Chistochina and Juneau have been passed through a power-line harmonic-interference-removal filter (Chistochina and Juneau have very little hum in the receiver).

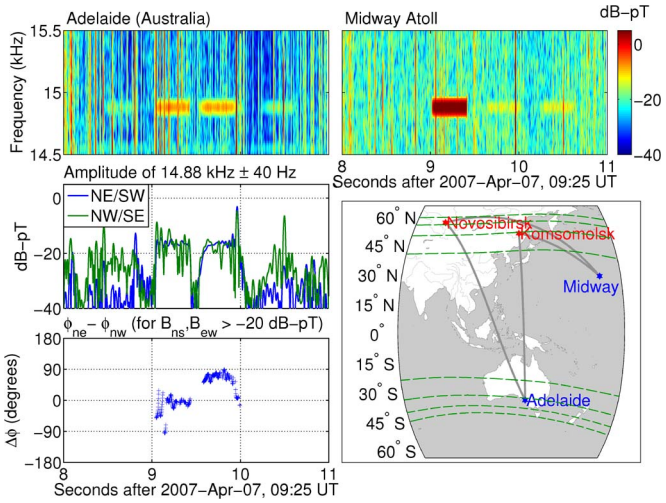

Fig. 12. Detection of magnetospherically propagating signals from VLF transmitters. (Bottom right panel) Two transmitters in Komsomolsk and Novosibirsk, which form two-thirds of the Alpha network, along with receivers at Midway and Adelaide. The Adelaide receiver is very close to the geomagnetic conjugate point of Komsomolsk. (Top panels) Spectrograms showing the received signal from the three Russian Alpha transmitters at 14.88 kHz, over a 3-s period on April 7, 2007. In particular, the two pulses received at Adelaide between seconds 9 and 10 are roughly the same amplitude, whereas at Midway, the second pulse is substantially weaker. Nominally, the first pulse is from Komsomolsk and the second is from Novosibirsk, but at Adelaide, the Novosibirsk pulse is in fact swamped by the presence of a second arrival from the same Komsomolsk transmitter. This is determined to be due to the magnetospherically propagating component of the first pulse, which arrives at the geomagnetic conjugate point of the transmitter, near Adelaide, but is not present at Midway. (Center left panel) Amplitude of 14.88 kHz detected at Adelaide, extracted over this 3-s period. The second pulse exhibits different characteristics than the first, i.e., a more gradual ON and OFF time. This is consistent with magnetospheric growth of the transmitter signal along the path. The lower left panel shows the phase difference between the two antenna channels. The first pulse shows no phase shift between the two, consistent with linearly polarized signal propagating in the Earth-ionosphere waveguide. However, the second pulse exhibits a phase shift of close to 90°, consistent with a signal arriving from the magnetosphere with circular polarization.

the HAARP input power was increased from 960 kW to 3.6 MW, which also increased the generated ELF signal strengths. Fig. 10 shows exceptionally strong signals received at Midway, up to -32 dB · pT (or ∼200 times more power than the original detection of HAARP signals at Midway). These signal levels are strong enough to be easily detected in a spectrogram, so that the signal strength can be tracked on a seconds-long timescale over a long period (in this case, 40 min long), as shown in the lower left panel of Fig. 10. The signal received at the receiver is therefore a diagnostic both of the directionality and strength of the ionospheric source above HAARP, as well as the ionospheric paths in between HAARP and the various receivers.

D. Magnetospheric Signals

A network of AWESOME receivers at high latitudes also enables simultaneous detection of magnetospherically generated signals, such as chorus. Fig. 11 shows a 15-s segment of data at five different AWESOME receivers across Alaska, spanning a wide range of L-shells (between 3.5 and 6) and longitudes, on February 15, 2007, 0105 UT. Due to the noise levels at Yakutat and the fact that only a small antenna is used there, the detection threshold is substantially higher than the other sites, but the chorus activity is nonetheless detected. The hum-subtraction filter described earlier is applied to Yakutat, Valdez, and Kodiak in order to mitigate the noise levels generated by 60-Hz harmonic radiation.

This case is analyzed more thoroughly by Gołkowski and Inan [21]. However, a simple comparison of the spectrograms reveals that this particular chorus activity was widespread both in geomagnetic latitude and longitude, being received simultaneously at all five sites. On the other hand, the individual chorus elements differ in terms of which site detects them with the highest amplitude. For instance, the most visible chorus element at Kodiak, at ∼01:05:55 UT, does not correspond with the strongest chorus elements at Valdez (at ∼01:05:50 UT and ∼01:05:58 UT), which is at a similar longitude but a higher latitude. However, the chorus activity at Juneau, Valdez, and Yakutat, which are at nearly identical geomagnetic latitudes seem to correspond quite well with each other. Gołkowski and Inan [21] attributed these observations to multiple exit points from the magnetosphere, after using methods to geolocate these magnetospheric exit points via direction finding and time of arrival.

Whistler-mode signals can also originate from man-made sources, such as VLF transmitters [61] and modulated HF heating of the auroral electrojet [62], [63]. The key difference between whistler-mode signals and signals propagating in the Earth-ionosphere waveguide is the polarization, with the former being largely circularly polarized, while the latter is largely linearly polarized. The use of two orthogonal antennas causes subionospherically propagating signals to be clearly distinguished from magnetospherically propagating signals reentering the Earth-ionosphere cavity. Fig. 12 shows one such instance from a receiver placed in Adelaide, Australia

(34.62° S, 138.46° E), within 100 km of the geomagnetic conjugate point of an "Alpha" VLF transmitter, as shown in the map on the bottom right panel of Fig. 12. We note that these magnetospheric signals propagate at much lower latitudes ($L \sim 1.95$) than the magnetospheric signals excited from the Siple Station Antarctic transmitter [15] at $L \sim 6$ and the HAARP HF heating facility [63] at $L \sim 4.9$. The Russian "Alpha" network consists of three transmitters across Russia, at Komsomolsk (50.07° N, 38.16° E), Novosobirsk (55.76° N, 4.45° E), and Krasnodar (45.40° N, 38.16° E), each of which alternates between three different CW frequencies, so that navigation is made possible via triangulation using the phase measurements. The top two panels show a series of four pulses at ∼14.85 kHz, each with 400-ms length and separated by 200 ms and originating from Krasnodar, Komsomolsk, Novosibirsk, and Novosibirsk, respectively, and in that order, both at Adelaide and at Midway Atoll. The Krasnodar pulse is too weak at Midway to be detected, but all the others can be distinguished in the spectrogram. In the Adelaide spectrogram, the first of the two Novosibirsk pulses is clearly overwhelmed by a signal ∼20 dB stronger superimposed onto it (whereas at Midway, where only the subionospheric signal is present, the two Novosibirsk pulses are not surprisingly of the same amplitude).

The phase accuracy of the signal detection enables us to explain this result as the arrival of the pulse from Komsomolsk via propagating in the whistler mode along a magnetospheric duct, so that its arrival via this slower mode of propagation nearly coincides with the arrival of the subionospheric pulse from Novosibirsk, i.e., a delay of ∼600 ms with respect to the subionospheric signal. The bottom left panel of Fig. 12 shows how the two-channel nature of the AWESOME enables unambiguous distinction between these two types of signal, by measuring the phase difference between the north–south and east–west antenna signals after digitally extracting the amplitude of a frequency band at 14.88 kHz ± 40 Hz. We note that a threshold of -25 dB · pT is applied for the phase calculations so that only reliable measurements are shown. The subionospherically propagating signal shows little or no phase difference between the two channels, indicative of a linearly polarized wave. Subionospheric signals detected at long distances often consist of only a small number of Earth-ionosphere modes, being dominated by those with low attenuation, so that the receiver signal consists of linear polarization. However, whistler-mode signals propagating in the magnetosphere propagate with right-hand circular polarization. The magnetospherically propagating pulse clearly shows a nearly 90° phase difference. Analysis of a $>$ 7-day period in early April 2007 shows periods of very high occurrences of one hops lasting on the order of a couple hours, which may also be connected to the K_p index.

Furthermore, the narrowband extracted amplitude shown in the right center panel indicates some characteristics known to accompany ducted wave propagation in the magnetosphere, such as a growth phase and a saturation phase, believed to be due to interactions in the magnetosphere between the wave and radiation-belt particles [64]. It is interesting to note that even though only a small fraction of the VLF energy is absorbed into the magnetosphere, the amplitude of the magnetospherically propagating signal is nearly the same as the subionospheric signal. The 500–600-ms propagation delay of the magnetospherically propagating signal implies a group velocity of 0.10–0.15 c, since a centered dipole assumption for the Earth's magnetic field yields a path length of ∼2.2 Mm. This is consistent with the typical speeds of whistler-mode propagation in the magnetosphere. Long-term analysis of these midlatitude magnetospheric signals enable a better understanding of both the evolving magnetospheric conditions, like the availability of ducts and the nature of the wave–particle interactions that drive the growth. The nature of these processes are relatively poorly understood for lower latitude sites, where the propagation paths are shorter, the magnetosphere is much more stable in the face of geomagnetic disturbances, the equatorial region (and therefore the growth region) is shorter, and the availability of ducts are likely different in general. Triggered emissions as have been observed with high-latitude ducted magnetospheric signals [3] may also be observed at these midlatitude sites.

X. Conclusion

A new instrument has been developed and deployed for sensitive reception of broadband ELF (300–3000 Hz) and VLF (3–30 kHz) radio signals from natural and man-made sources, based on existing designs used for decades at Stanford University. We describe the performance characteristics of the AWESOME instrument, including sensitivity, frequency and phase response, timing accuracy, and cross modulation. We also described a broad range of scientific applications as used by AWESOME ELF/VLF data, involving measurements of both subionospherically and magnetospherically propagating signals of both natural and man-made variety.

We also noted that the AWESOME receivers have been distributed under the auspices of the International Heliophysical Year (IHY), for the purpose of scientific capacity building and educational outreach. A joint space weather monitor program, including both the AWESOME receiver and a simpler version known as the SID, is described by [65].

Acknowledgment

The authors would like to thank J. Tan, E. Kim, J. Chang, R. Said, M. Gołkowski, and J. Payne for significant help in development of the AWESOME receiver. They would also like to thank R. Moore and E. Kim for developing the recording software. They would also like to thank P. Scherrer and D. Scherrer for their support. They would also like to thank J. Davila for his support under the IHY program and D. Byers.

References

[1] M. A. Uman, *The Lightning Discharge*. New York: Dover, 1987.
[2] K. Davies, *Ionospheric Radio*. Stevenage, U.K.: Inst. Eng. Technol., 1990.
[3] R. A. Helliwell, "VLF wave-injection experiments from Siple Station, Antarctica," *Adv. Space Res.*, vol. 8, no. 1, pp. 279–289, 1988.
[4] M. Platino, U. S. Inan, T. F. Bell, J. S. Picket, and P. Canu, "Rapidly moving sources of upper band ELF/VLF chorus near the geomagnetic equator," *J. Geophys. Res.*, vol. 111, no. A9, p. A09 218, Sep. 2006. DOI:10.1029/2005JA011468.
[5] E. R. Swanson, "Omega," *Proc. IEEE*, vol. 71, no. 10, pp. 1140–1155, Oct. 1983.

[6] J. D. Mcneil and V. F. Labson, "Geological mapping using VLF radio field," in *Electromagnetic Methods in Applied Geophysics*, vol. 2. Tulsa, OK: Soc. Explor. Geophys., 1991, ch. 7.

[7] R. A. Helliwell, *Whistlers and Related Ionospheric Phenomena*. New York: Dover, 1965.

[8] F. W. Chapman, D. D. Jones, J. D. W. Todd, and R. A. Challinor, "Observations on the propagation constant of the Earth-ionosphere waveguide in the frequency band 8 c/s to 16 kc/s," *Radio Sci.*, vol. 11, pp. 1273–1282, Nov. 1966.

[9] K. Budden, *The Wave-Guide Mode Theory of Wave Propagation*. Moscow, ID: Logos Press, 1961.

[10] J. R. Wait, *Electromagnetic Waves in Stratified Media*. New York: Pergamon, 1962.

[11] R. K. Potter, "Analysis of audio-frequency atmospherics," *Proc. IRE*, vol. 39, no. 9, pp. 1067–1069, Sep. 1951.

[12] E. W. Paschal, "The design of broad-band VLF receivers with air-core loop antennas," STARLab, Stanford Univ., Stanford, CA, 1980. Tech. Rep.

[13] R. A. Helliwell, "Low frequency propagation studies: Part I," in "Whistlers and Related Phenomena Final Report," Stanford Radio Propag. Lab., Stanford Univ., Stanford, CA, Air Force Contract AF19(604)-795, AFCRC-TR-56-189, 1956.

[14] R. Raghuram, R. L. Smith, and T. F. Bell, "VLF antarctic antenna: Impedance and efficiency," *IEEE Trans. Antennas Propag.*, vol. AP-22, no. 2, pp. 334–338, Mar. 1974.

[15] R. A. Helliwell and J. P. Katsufrakis, "VLF wave injection into the magnetosphere from Siple Station, Antarctica," *J. Geophys. Res.*, vol. 79, no. 16, pp. 2511–2518, 1974.

[16] E. W. Paschal, "Phase measurements of very low frequency signals from the magnetosphere," Ph.D. dissertation, Stanford Univ., Stanford, CA, 1988.

[17] A. C. Fraser-Smith and R. A. Helliwell, "The Stanford University ELF/VLF radiometer project: Measurement of the global distribution of ELF/VLF electromagnetic noise," in *Proc. IEEE Int. Symp. Electromagn. Compat.*, 1985, pp. 305–311.

[18] A. C. Fraser-Smith, R. A. Helliwell, P. R. Fortnam, B. R. andMcGill, and C. C. Teague, "A new global survey of ELF/VLF radio noise," in *Proc. NATO/AGARD Conf.—Effects of Electromagnetic Noise and Interference on Performance of Military Radio Communication Systems*, Lisbon, Portugal, 1987.

[19] D. A. Chrissan and A. C. Fraser-Smith, "Seasonal variations of globally measured ELF/VLF radio noise," *Radio Sci.*, vol. 31, no. 5, pp. 1141–1152, 1996.

[20] S. K. Harriman, E. W. Paschal, and U. S. Inan, "Magnetic sensor design for femto-tesla low-frequency signals," *IEEE Trans. Geosci. Remote Sens.*, vol. 47, no. 12, Dec. 2009, to be published.

[21] M. Gołkowski and U. S. Inan, "Multistation observations of ELF/VLF whistler mode chorus," *J. Geophys. Res.*, vol. 113, no. A8, p. A08 210, Aug. 2008. DOI:10.1029/2007JA012977.

[22] M. Hayakawa and S. S. Sazhin, "Mid-latitude and plasmaspheric hiss—A review," *Planet. Space Sci.*, vol. 40, no. 10, pp. 1325–1338, Oct. 1992.

[23] M. B. Cohen, M. Gołkowski, and U. S. Inan, "Orientation of the HAARP ELF ionospheric dipole and the auroral electrojet," *Geophys. Res. Lett.*, vol. 35, no. 2, p. L02 806, Jan. 2008. DOI:10.1029/2007GL032424.

[24] T. G. Wolf and U. S. Inan, "Path-dependent properties of subionospheric VLF amplitude and phase perturbations associated with lightning," *J. Geophys. Res.*, vol. 95, no. A12, pp. 20 997–21 005, 1990.

[25] U. S. Inan, "VLF heating of the lower ionosphere," *Geophys. Res. Lett.*, vol. 17, no. 6, pp. 729–732, May 1990.

[26] U. S. Inan, M. Gołkowski, M. K. Casey, R. C. Moore, W. Peter, P. Kulkarni, P. Kossey, E. Kennedy, S. Z. Meth, and P. Smit, "Subionospheric VLF observations of transmitter-induced precipitation of inner radiation belt electrons," *Geophys. Res. Lett.*, vol. 34, no. 2, p. L02 106, Jan. 2007. DOI:10.1029/2006GL028494.

[27] J. V. Rodriguez and U. S. Inan, "Electron density changes in the nighttime D region due to heating by very-low-frequency transmitters," *Geophys. Res. Lett.*, vol. 21, no. 2, pp. 93–96, 1994.

[28] T. B. Jones, K. Davies, and B. Wieder, "Observations of D-region modifications and low and very low frequencies," *Nature*, vol. 238, no. 5358, pp. 33–34, Jul. 1972.

[29] R. Barr, M. T. Rietveld, P. Stubbe, and H. Kopka, "The diffraction of VLF radio waves by a patch of ionosphere illuminated by a powerful HF transmitter," *J. Geophys. Res.*, vol. 90, no. A3, pp. 2861–2875, Mar. 1985.

[30] R. C. Moore, "ELF/VLF wave generation by modulated HF heating of the auroral electrojet," Ph.D. dissertation, Stanford Univ., Stanford, CA, 2007.

[31] T. G. Wood and U. S. Inan, "Long-range tracking of thunderstorms using sferic measurements," *J. Geophys. Res.*, vol. 107, no. D21, p. 4553, Nov. 2002.

[32] S. A. Cummer, U. S. Inan, and T. Bell, "Ionospheric D region remote sensing using VLF radio atmospherics," *Radio Sci.*, vol. 33, no. 6, pp. 1781–1792, 1998.

[33] M. A. Clilverd, N. R. Thomson, and C. J. Rodger, "Sunrise effects on VLF signals propagating over a long north–south path," *Radio Sci.*, vol. 34, no. 4, pp. 939–948, 1999.

[34] H. J. Christian, R. J. Blakeslee, D. J. Boccippio, W. L. Boeck, D. E. Buechler, K. T. Driscoll, S. J. Goodman, J. M. Hall, W. J. Koshak, D. M. Mach, and M. F. Stewart, "Global frequency and distribution of lightning as observed from space by the optical transient detector," *J. Geophys. Res.*, vol. 108, no. D1, p. 4005, Jan. 2003.

[35] U. S. Inan, M. B. Cohen, R. K. Said, D. M. Smith, and L. I. Lopez, "Terrestrial gamma ray flashes and lightning discharges," *Geophys. Res. Lett.*, vol. 33, no. 18, p. L18 802, Sep. 2006. DOI:10.1029/2006GL027085.

[36] G. J. Fishman, P. N. Bhat, R. Mallozzi, J. M. Horack, T. Koshut, C. Kouveliotou, G. N. Pendleton, C. A. Meegan, R. B. Wilson, and W. S. Paciesas, "Discovery of intense gamma-ray flashes of atmospheric origin," *Science*, vol. 264, no. 5163, pp. 1313–1316, May 1994.

[37] D. M. Smith, L. I. Lopez, R. P. Lin, and C. P. Barrington-Leigh, "Terrestrial gamma-ray flashes observed up to 20 MeV," *Science*, vol. 308, no. 5712, pp. 1085–1088, Feb. 2005.

[38] U. S. Inan, S. C. Reising, G. J. Fishman, and J. M. Horack, "On the association of terrestrial gamma-ray bursts with lightning and implications for sprites," *Geophys. Res. Lett.*, vol. 23, no. 9, pp. 1017–1020, May 1996.

[39] M. B. Cohen, U. S. Inan, and G. R. Fishman, "Terrestrial gamma ray flashes observed aboard Compton Gamma Ray Observatory/Burst and Transient Source Experiment and ELF/VLF radio atmospherics," *J. Geophys. Res.*, vol. 111, no. D24, p. D24 109, Dec. 2006. DOI:10.1.1029/2005JD006987.

[40] T. G. Wood and U. S. Inan, "Localization of individual lightning discharges via directional and temporal triangulation of sferic measurements and two distant sites," *J. Geophys. Res.*, vol. 109, no. D21, p. D21 109, Nov. 2004. DOI:10.1029/2004JD005204.

[41] Y. N. Taranenko, U. S. Inan, and T. F. Bell, "Interaction with the lower ionosphere of electromagnetic pulses from lightning: Heating, attachment, and ionization," *Geophys. Res. Lett.*, vol. 20, no. 15, pp. 1539–1542, Aug. 1993.

[42] W. B. Peter and U. S. Inan, "A quantitative comparison of lightning-induced electron precipitation and VLF signal perturbations," *J. Geophys. Res.*, vol. 112, no. A12, p. A12 212, Dec. 2007. DOI:10.1029/2006JA012165.

[43] S. A. Cummer, T. F. Bell, U. S. Inan, and D. L. Chenette, "VLF remote sensing of high-energy auroral particle precipitation," *J. Geophys. Res.*, vol. 102, no. A4, pp. 7477–7484, 1997.

[44] U. S. Inan, T. F. Bell, V. P. Pasko, D. D. Sentman, E. M. Wescott, and W. A. Lyons, "VLF signatures of ionospheric disturbances associated with sprites," *Geophys. Res. Lett.*, vol. 22, no. 24, pp. 3461–3464, 1995.

[45] A. P. Mitra, *Ionospheric Effects of Solar Flares*. Dordrecht, The Netherlands: Reidel, 1974.

[46] C. J. Rodger, M. A. Clilverd, N. R. Thomson, R. J. Gamble, A. Sappala, E. Turunen, N. P. Meredith, M. Parrot, J. A. Sauvaud, and J. J. Berthelier, "Radiation belt electron precipitation into the atmosphere: Recovery from a geomagnetic storm," *J. Geophys. Res.*, vol. 112, no. A11, p. A11 307, Nov. 2007. DOI:10.1029/2007JA012383.

[47] M. A. Clilverd, C. J. Rodger, and N. R. Thomson, "Investigating seismoionospheric effects on a long subionospheric path," *J. Geophys. Res.*, vol. 104, no. A12, pp. 28 171–28 179, 1999.

[48] U. S. Inan, N. G. Lehtinen, S. J. Lev-Tov, M. P. Johnson, T. F. Bell, and K. Hurley, "Ionization of the lower ionosphere by γ-rays from a magnetar: Detection of a low energy (3–10 keV) component," *Geophys. Res. Lett.*, vol. 26, no. 22, pp. 3357–3360, 1999.

[49] M. A. Clilverd, C. J. Rodger, N. R. Thomson, J. Lichtenberger, P. Steinback, P. Cannon, and M. J. Angling, "Total solar eclipse effects on VLF signals: Observations and modeling," *Radio Sci.*, vol. 36, no. 4, pp. 773–788, 2001.

[50] G. J. Fishman and U. S. Inan, "Observation of an ionospheric disturbance caused by a gamma-ray burst," *Nature*, vol. 331, no. 6155, pp. 418–420, Feb. 1988.

[51] U. S. Inan, A. Slingeland, V. P. Pasko, and J. V. Rodriguez, "VLF and LF signatures of mesospheric/lower ionospheric response to lightning discharges," *J. Geophys. Res.*, vol. 101, no. A3, pp. 5219–5238, Mar. 1996.

[52] C. Haldoupis, T. Neubert, U. S. Inan, A. Mika, T. H. Allin, and R. A. Marshall, "Subionospheric early VLF signal perturbations

observed in one-to-one association with sprites," *J. Geophys. Res.*, vol. 109, no. A10, p. A10 303, Oct. 2004. DOI:10.1029/2004JA010651.
[53] R. Marshall, R. Newsome, and U. Inan, "Fast photometric imaging using orthogonal linear arrays," *IEEE Trans. Geosci. Remote Sens.*, vol. 46, no. 11, pp. 3885–3893, Nov. 2008.
[54] M. P. Johnson, U. S. Inan, S. J. Lev-Tov, and T. F. Bell, "Scattering pattern of lightning-induced ionospheric disturbances associated with early/fast VLF events," *Geophys. Res. Lett.*, vol. 26, no. 15, pp. 2363–2366, Aug. 1999.
[55] D. L. Jones, "ELF radio," in *Proc. Int. Conf. 100 Years Radio*, 1995, vol. 141, pp. 101–106.
[56] C. G. Getmantsev, N. A. Zuikov, D. S. Kotik, N. A. Mironenko, V. O. Mityakov, Y. A. Rapoport, V. Y. Sazanov, V. Y. Trakhtengerts, and V. Y. Eidman, "Combination frequencies in the interaction between high-power short-wave radiation and ionospheric plasma," *JETP Lett.*, vol. 20, pp. 101–102, Aug. 1974.
[57] P. H. Stubbe, H. Kopka, M. T. Rietveld, and R. L. Dowden, "ELF and VLF generation by modulated heating of the current carrying ionosphere," *J. Atmos. Terr. Phys.*, vol. 44, no. 12, pp. 1123–1135, 1982.
[58] D. H. Werner and A. J. Ferraro, "Steerable ELF/VLF radiation produced by an array of ionospheric dipoles generated from HF heating," *IEEE Trans. Antennas Propag.*, vol. AP-35, no. 9, pp. 1022–1030, Sep. 1987.
[59] R. C. Moore, U. S. Inan, T. F. Bell, and E. J. Kennedy, "ELF waves generated by modulated HF heating of the auroral electrojet and observed at a ground distance of ∼4400 km," *J. Geophys. Res.*, vol. 112, no. A5, p. A05 309, May 2007. DOI:10.1029/2006JA012063.
[60] M. B. Cohen, U. S. Inan, and M. Gołkowski, "Geometric modulation: A more effective method of steerable ELF/VLF wave generation with continuous HF heating of the lower ionosphere," *Geophys. Res. Lett.*, vol. 35, no. 12, p. L12 101, Jun. 2008. DOI:10.1029/2008GL034061.
[61] N. R. Thomson, "Whistler mode signals: Spectrographic group delays," *J. Geophys. Res.*, vol. 86, no. A6, pp. 4795–4802, Jun. 1981.
[62] U. S. Inan, M. Gołkowski, D. L. Carpenter, N. Reddell, R. C. Moore, T. F. Bell, E. W. Paschal, P. Kossey, E. Kennedy, and S. Z. Meth, "Multi-hop whistler-mode ELF/VLF signals and triggered emissions excited by the HAARP HF heater," *Geophys. Res. Lett.*, vol. 31, no. 24, p. L24 805, Dec. 2004. DOI:10.1029/2004GL021647.
[63] M. Gołkowski, U. S. Inan, A. R. Gibby, and M. B. Cohen, "Magnetospheric amplification and emission triggering by ELF/VLF waves injected by the 3.6 MW HAARP ionospheric heater," *J. Geophys. Res.*, vol. 113, no. A10, p. A10 201, Oct. 2008. DOI:10.1029/2008JA013157.
[64] A. R. Gibby, U. S. Inan, and T. F. Bell, "Saturation effects in the VLF-triggered emission process," *J. Geophys. Res.*, vol. 113, no. A11, p. A11 215, Nov. 2008. DOI:10.1029/2008JA013233.
[65] D. Scherrer, M. Cohen, T. Hoeksema, U. Inan, R. Mitchell, and P. Scherrer, "Distributing space weather monitoring instruments and educational materials worldwide for IHY 2007: The AWESOME and SID project," *Adv. Space Res.*, vol. 42, no. 11, pp. 1777–1785, Dec. 2008.

Morris B. Cohen (S'09–M'09) received the B.S., M.S., and Ph.D. degrees in electrical engineering from Stanford University, Stanford, CA, in 2003, 2004, and 2009, respectively.

He is currently with the Space, Telecommunications, and Radioscience Laboratory, Department of Electrical Engineering, Stanford University. He also serves as the Coordinator of Stanford's Research Experience for Undergraduates Summer Internship Program and the International Scientific Outreach Manager under Stanford's Atmospheric Weather Electromagnetic System for Observation, Modeling, and Education (AWESOME) global instrument network, in coordination with the International Heliophysical Year and the United Nations Basic Space Science Initiative. His research interests include nonlinear interactions of high-frequency radio waves with the lower ionosphere, extremely low frequency/very low frequency (ELF/VLF) radio-wave propagation in the ionosphere and magnetosphere, lightning-generated radio atmospherics and terrestrial gamma-ray flashes, and ELF/VLF radio instrumentation.

Dr. Cohen was the recipient of an American Geophysical Union Outstanding Student Paper Award in Fall 2005 and Fall 2007, and a Top-5 Award in the 2008 International Union of Radio Science International Student Paper Competition.

Umran S. Inan (S'76–M'77–SM'99–F'06) received the B.S. and M.S. degrees in electrical engineering from Middle East Technical University, Ankara, Turkey, in 1972 and 1973, respectively, and the Ph.D. degree in electrical engineering from Stanford University, Stanford, CA, in 1977.

He is currently with Stanford University, as a Professor of electrical engineering with the Department of Electrical Engineering and the Director of the Space, Telecommunications, and Radioscience Laboratory. He is also currently the President of Koç University, Istanbul, Turkey. He actively conducts research on electromagnetic waves in plasmas, lightning discharges, ionospheric physics, near-Earth space physics, radiation belts, and very low frequency remote sensing. Since 1990, he has been serving as the Principal Ph.D. Dissertation Advisor for 32 students who have received their degrees.

Dr. Inan is a Fellow of the American Geophysical Union and is a member of Tau Beta Pi, Sigma Xi, and the Electromagnetics Academy. He has served as the Chair of the U.S. National Committee of the International Union of Radio Science (URSI) and the International Chair of Commission H (Waves in Plasmas) of URSI. He is currently serving as the Vice President of URSI. He was the recipient of the 2007 Stanford University Allan V. Cox Medal for Faculty Excellence in Fostering Undergraduate Research; the 1998 Stanford University Tau Beta Pi Award for Excellence in Undergraduate Teaching; several Group Achievement Awards from the National Aeronautics and Space Administration and the European Space Agency; the Antarctic Service Medal of the U.S., with an Antarctic Mountain named "Inan Peak" in his honor; and the 2008 Appleton Prize from URSI and the Royal Society.

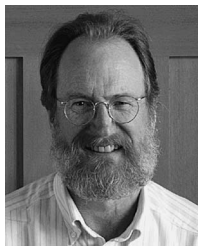

Evans W. Paschal received the B.A. degree in physics from Reed College, Portland, OR, in 1968 and the M.S. and Ph.D. degrees in electrical engineering from Stanford University, Stanford, CA, in 1969 and 1988, respectively. His Ph.D. degree is focused on the study of phase characteristics of magnetospheric whistler-mode signals from the very low frequency (VLF) transmitter at Siple Station, Antarctica.

From 1976 to 1986, he was a Research Associate in the VLF Group of the Space, Telecommunications, and Radioscience Laboratory, Stanford University. In 1992, he started Whistler Radio Services, a consulting business on Anderson Island, WA. He has 40 years of experience in the design and operation of instruments for magnetospheric research. He has developed novel broadband extremely low frequency and VLF radio receivers and computerized recording and signal-analysis equipment. He has made numerous trips to field stations in Antarctica and elsewhere in support of this research.

Dr. Paschal is a member of the American Geophysical Union, Sigma Xi, and the American Association for the Advancement of Science.